EFDA–JET–PR(10)43

M. Honda, T. Takizuka, K. Tobita, G. Matsunaga, A. Fukuyama
and JET EFDA contributors

Alpha Particle-Driven Toroidal Rotation in Burning Plasmas

Alpha Particle-Driven Toroidal Rotation in Burning Plasmas

M. Honda[1], T. Takizuka[1], K. Tobita[1], G. Matsunaga[1], A. Fukuyama[2]
and JET EFDA contributors*

JET-EFDA, Culham Science Centre, OX14 3DB, Abingdon, UK

[1]Japan Atomic Energy Agency, Naka, Ibaraki 311-0193, Japan
[2]Department of Nuclear Engineering, Kyoto University, Kyoto 606-8501, Japan
** See annex of F. Romanelli et al, "Overview of JET Results",*
(23rd IAEA Fusion Energy Conference, Daejon, Republic of Korea (2010)).

Preprint of Paper to be submitted for publication in
Nuclear Fusion

ABSTRACT.
The mechanism of a torque intrinsically produced by alpha particles and the subsequent possibility to create significant toroidal rotation and shear are investigated. In DEMO plasmas, the orbit-following Monte Carlo code OFMC predicts that co-directed collisional torque and a counter-directed $\vec{j} \times \vec{B}$ torque always emerge regardless of the magnetic configuration, and both of them virtually cancel each other out. It is found that the gradient of the source profile of alpha particles produces both torques, and the magnitude of each torque is enhanced in the reversed shear configuration compared to the normal shear configuration, provided that the source gradient is finite and similar in both cases. The resultant rotation velocity estimated by the TASK/TX transport code is far below the threshold to stabilize resistive wall modes through intrinsic alpha-driven torque alone. It is estimated that a neutral beam injection at a moderate power level may be necessary for obtaining toroidal rotation sufficient to stabilize resistive wall modes.

1. INTRODUCTION

Toroidal rotation and shear play an important role in suppressing turbulent transport and MHD instabilities not only in current tokamak plasmas but also in burning plasmas for ITER and DEMO. In current devices toroidal rotation can be driven and controlled with a tangentially-injected Neutral Beam (NB) through a collisional slowing-down momentum transfer process involving passing particles. However, we will have limited means to drive and control toroidal rotation in DEMO, where self-generated alpha particle heating will be dominant. Therefore, only a few external heating systems may be expected to be installed; port openings for these systems in a vacuum vessel take up space that potentially reduces the tritium breeding ratio below unity, indicating that a self-sufficient, fuel-generating plasma is no longer feasible. In addition, collisional momentum transfer from tangential NBIs would not be significant in the core region of a DEMO plasma: first, the beam energy Eb is higher than that used in current devices, such that the momentum input expressed by $\sim P_b/E_b^{1/2}$ [1] becomes smaller, where P_b denotes the beam power. In SlimCS [2], one of the DEMO concepts, in addition to an electron cyclotron heating system, a negative-ion-based Neutral Beam Injection (NBI) system is planned to be installed, and $E_b \sim 0.5-1.5$MeV is expected, which is around 5–20 times higher than that of positive ion-based NBIs. Secondly, the high density of the plasma results in a short mean free path of beam ions. These beam ions are likely to be trapped in the outboard region of the plasma, leading to a decrease in the number of passing particles in the core region. In this sense, in order to evaluate the impact of toroidal rotation on turbulence and MHD instability, we first explore the potential of an intrinsic torque source in self-sustained, burning plasmas.

In this paper we focus on torque and toroidal rotation stemming solely from alpha particles despite several other possible intrinsic torque sources in burning plasmas. To our knowledge, only a few papers discuss alpha-driven toroidal rotation and/or torque [3, 4, 5, 6]. Rosenbluth and Hinton, analytically solving equations of motion and Fokker- Planck equations for extreme cases, conclude that rotation and its shear sufficient to suppress instabilities may be impossible in a tokamak reactor

[4] because, in general, the frictional (collisional) and the $\vec{j} \times \vec{B}$ torques cancel out if the alpha orbits are well-confined. Schneider et al. illustrate that the $\vec{j} \times \vec{B}$ torque will be invoked by alpha particles [5], but the main body of their work focuses primarily on an alphadriven current, not rotation, similar to the work of Tani and Azumi [7]. Collisionless test-particle simulations with a Solov'ev equilibrium by Thyagaraja et al. clearly show that a positive (outward) fast-ion radial current does flow in ITER, pushing a bulk plasma in a direction counter to the plasma current [6]. As a result, they state that counter-current NBIs should be installed in ITER to enhance counter-toroidal rotation. However, their work ignores the contribution of collisional alpha-particle torque, which may offset collisionless torque, i.e., the $\vec{j} \times \vec{B}$ torque, as Rosenbluth and Hinton state [4].

Based on the preceding research, we now investigate an intrinsic torque stemming from the motion of alpha particles born from fusion reactions and the resulting toroidal rotation in SlimCS plasmas, using mainly the orbit-following Monte Carlo code OFMC [8] and partly the one-dimensional transport code TASK/TX [9]. A DEMO plasma with an Internal Transport Barrier (ITB) in a Weakly Reversed Shear (W-RS) configuration is generally anticipated to exist in a steady state because these conditions are necessary to sustain the high bootstrap current fraction that is essential for steady-state operations. Density and temperature profiles determine the birth profile of alpha particles, and alpha orbits conform to the magnetic configuration, both of which have a significant impact on the torque profile. In this sense, we have to consider reasonable conditions regarding the magnetic configuration and the source profile of alpha particles of a DEMO plasma, a focus which clearly distinguishes our study from preceding work.

The rest of this paper is organized as follows. The characteristics of alpha particle orbits are briefly described in section 2 with an emphasis on those characteristics which are peculiar to alpha particles, unlike beam particles. In section 3, a method to compute the $\vec{j} \times \vec{B}$ torque in OFMC and a benchmark test for estimating torque using OFMC and the ASCOT code [10] are described. The physical characteristics of alpha particleinduced torque are characterized in detail in section 4. Section 5 is devoted to predictive simulations of torques and toroidal rotation produced by alpha particles in SlimCS. The torque produced by a tangential NBI is also estimated. Finally, conclusions and discussion are given in section 6.

2. ALPHA PARTICLE ORBIT

In burning plasmas with deuterium and tritium mixed, alpha particles are constantly born due to D-T fusion reactions. This process actually creates no electrons, unlike the ionization of fast neutrals by NBIs: collisions between ionized deuterium and tritium produce a charged alpha particle, i.e., a fast helium ion, and a neutron. In terms of quasineutrality, however, we may regard the two electrons adjacent to the fusion reaction as ones which accompany the fusion reaction, because they practically offset the charges of the deuterium and tritium ions. These electrons remain at the surface where the reaction occurs, while a fusion-born alpha particle deviates from the surface due to drift motion. The maximum deviation of a particle is about $\sim \in^{1/2} \rho_\theta$ for trapped particles

and $\sim \in\rho_\theta$ for passing ones, where $\in$ is the inverse aspect ratio and ρ_θ, the poloidal Larmor radius. Because ρ_θ is proportional to $T_i^{1/2}$ and inversely proportional to B_θ, where T_i is the ion temperature and B_θ, the poloidal magnetic field, we expect that a trapped alpha particle with 3:5MeV in the core region of a Reversed Shear (RS) plasma has a deviation width much wider than those of any other particle. This charge separation between alpha particles and electrons must generate a fast-ion radial current. Owing to the large dielectric constant of a fusion plasma, an opposite radial current driving toroidal rotation emerges in the plasma [4]. Unlike directional NBIs, however, alpha particles are isotropically born at the moment of their birth in general. This fact suggests that it is not straightforward to determine the direction of the $\vec{j} \times \vec{B}$ torque or whether the torque integrated over the entire volume is finite or not. A similar case holds for collisional torque. Isotropic birth means that particles are born with an equal probability of having any pitch angle. The likely result may seem at first to be no net collisional torque as a whole.

When considering finite orbit widths and the parabolic source profile of alpha particles, however, we anticipate finite collisional and $\vec{j} \times \vec{B}$ torques; in other words, alpha particles have directional characteristics. The preceding analytical studies clarify that the trapping boundary is asymmetric in a parallel velocity $V_{\|}$ near the magnetic axis [11], indicating that the trapping ratio for particles with a negative $V_{\|}$ is higher than that for particles with a positive $V_{\|}$, and that a trapping boundary ceases to exist for co-moving particles with sufficiently high energies [12]. These studies indicate that co-passing alpha particles are predominant, at least near the magnetic axis, due to the finite orbit-width effect. Numerical analyses of alpha particles in JET also show an excess of co-passing particles relative to counter-passing ones [13]. The source of alpha particles is proportional to the square of both density and temperature of a bulk plasma, so that the profile is centrally peaked and localized in the core region. In other words, particles born on a surface outnumber those born on any outward adjacent surface in the core region. This gradient of the source profile leads to a co-directed particle flow and an outward fast-ion radial current due to the finite-orbit-width effect. These issues concerning the orbit of alpha particles will be considered in detail in the following sections using numerical simulations.

3. MODELLING THE $\vec{j} \times \vec{B}$ TORQUE ESTIMATED BY OFMC

OFMC was recently updated to enable estimation of the $\vec{j} \times \vec{B}$ torque, as well as collisional torque. In this section, a method to compute the $\vec{j} \times \vec{B}$ torque in OFMC is described in detail.

3.1. A METHOD TO ESTIMATE THE $\vec{j} \times \vec{B}$ TORQUE

The radial current j_ψ and the resultant $\vec{j} \times \vec{B}$ torque occur due to a non-ambipolar charge separation, where the subscript ψ denotes the poloidal flux and the label of the flux surface. The charge separation can be regarded as a polarization in a dielectric plasma medium. In this sense, ionization of a neutral produces an electric dipole consisting of an electron-ion pair. The relationship between the induced polarization density $\vec{P}$ and the polarization charge density ρ_p is given by

$$\rho_p(\psi) = -\nabla \cdot \vec{P} \tag{1}$$

The induced polarization current $\vec{j}_p$ satisfies the law of conservation of charge, yielding

$$\nabla \cdot \vec{j}_p + \frac{\partial \rho_p}{\partial t} = 0 \tag{2}$$

Integrating (2) over the volume V after substituting (1) into it gives

$$\vec{j}_p = \frac{\partial \vec{P}}{\partial t}$$

clearly indicating that a non-ambipolar polarization current will continue to flow as long as polarization occurs due to the charge separation by NBI, for example.

Averaging (2) over the flux surface, we obtain

$$\left\langle \nabla \cdot \vec{j}_p \right\rangle = \frac{\partial}{\partial V} \left\langle \vec{j}_p \cdot \nabla V \right\rangle = -\frac{\partial \rho_p}{\partial t}$$

where we have adopted the formula for the flux surface-average. If we use the poloidal flux as the radial coordinate instead of V , we have

$$\frac{1}{V'} \frac{\partial}{\partial \psi} \left(V' \left\langle \vec{j}_p \cdot \nabla \psi \right\rangle \right) = -\frac{\partial \rho_p}{\partial t}$$

where $V' \equiv \partial V / \partial \psi$. Integrating this equation along the radial direction results in a local $\vec{j} \times \vec{B}$ torque as follows:

$$\left\langle \vec{j}_p \cdot \quad \psi \right\rangle = -\frac{1}{V'} \int_0^{\psi} V' \frac{\partial \rho_p}{\partial t} \, d\psi' \tag{3}$$

When we consider the toroidal, $R\hat{\zeta}$, projection of the flux surface-averaged equation of motion summed over the thermal species, a term related to the Lorentz force may have the form:D

$$\left\langle R\hat{\zeta} \cdot \vec{j} \times \vec{B} \right\rangle = \left\langle \vec{j} \cdot \nabla \psi \right\rangle$$

where $\vec{B} = \nabla\zeta \times \nabla\psi + I\nabla\zeta$ and $I(\psi) = RB_\zeta$. Here, j denotes the current composed of thermal plasma species other than fast-ion species. In fact, $\langle \vec{j} \cdot \nabla\psi \rangle$ is the torque density. In normal situations, a non-ambipolar radial current hardly emerges in a plasma due to quasi-neutrality and non-ambipolarity of neoclassical and anomalous transport, except in a transient phase, such that $\langle \vec{j} \cdot \nabla\psi \rangle$ is nil. However, once non-ambipolar charge separation occurs for some reason, the non-ambipolar component of the radial current emerging in a plasma produces a net $\vec{j} \times \vec{B}$ torque.

The relationship between the bulk-ion radial current and that of fast-ions is explained as follows.

When we average the radial component of Ampére's law over the flux surface, we have

$$\epsilon_0 \frac{\partial}{\partial t} \left\langle \vec{E} \cdot \nabla \psi \right\rangle + \left\langle \vec{j}^{\,tot} \cdot \nabla \psi \right\rangle = 0 \tag{4}$$

where $\in_0$ is the dielectric constant in a vacuum. Using the momentum equation and assuming that the plasma dielectric constant is large and valid for neoclassical plasmas, the first term of (4) is negligible [4, 14, 15], and hence D

$$\left\langle \vec{j}^{\,tot} \cdot \nabla \psi \right\rangle \simeq 0 \tag{5}$$

Considering $\vec{j}^{\,tot} \equiv \vec{j}^{\,plasma} + \vec{j}_p^{\,fast}$, the first of which is usually ambipolar and thus nil, and the latter of which is non-ambipolar, we finally obtain

$$\left\langle \vec{j} \cdot \nabla \psi \right\rangle \simeq - \left\langle \vec{j}_p \cdot \nabla \psi \right\rangle = \frac{1}{V'} \int_0^{\psi} V' \frac{\partial \rho_p}{\partial t} \, d\psi' = \frac{1}{\bar{V}'} \frac{\partial \psi}{\partial \bar{\rho}} \int_0^{\bar{\rho}} \bar{V}' \frac{\partial \rho_p}{\partial t} d\bar{\rho}, \tag{6}$$

applying (3) and (5). Here, ρ denotes the normalized minor radius and $\bar{V}' \equiv \partial \bar{V} / \partial \rho$. This is the actual equation adopted in OFMC to estimate the $\vec{j} \times \vec{B}$ torque.

In practice, OFMC estimates $\partial \rho_p / \partial t$ for each minute time increment, typically $\Delta t / \tau_s \sim 10^{-5}$ for beam particles and $\sim 10^{-6}$ for alpha particles, during the slowing down process. Here, τ_s represents the slowing down time. Because we assume that the accompanying electron remains at the flux surface where the ion is born, due to the very small Larmor radius of an electron, we are able to ascertain the distribution of accompanying electrons right after the birth of test particles. We, therefore, can compute a ρ_p profile for each test particle for each time increment by detecting the location of the test particle and then summing its charge and that of the accompanying electron on each flux surface. If we integrated ρ_p over the volume, we would expect a polarization density profile $\vec{P}$ according to (1), which would help us to understand the physics of charge separation. Further details regarding the practical estimation of ρ_p are described in Ref. [16].

3.2. A BENCHMARK TEST USING OFMC AND ASCOT

In order to test implementation of the mechanism for estimating the $\vec{j} \times \vec{B}$ torque, we carry out a benchmark test using OFMC and ASCOT [10]. An equilibrium as well as profiles of density and temperature are used from Pulse No: 72629 in JET at t = 50s. We artificially assume for this benchmark test only that 8 NBIs of the octant 8 neutral beam heating system (see figure 2 in [17]), with 100keV (mono-energy), 1MW each are activated and there are no toroidal field-ripple effects. OFMC uses 100, 000 test particles in total, while ASCOT uses 20, 000 test particles for each NBI, i.e., 160, 000 in total. We then compare both the collisional and $\vec{j} \times \vec{B}$ torque profiles after all test particles have been completely thermalized. A comparison of the torques is shown in figure 1, indicating that the OFMC and ASCOT results for both torques show good agreement. This agrement increases confidence in the reliability of both codes.

4. PHYSICS OF ALPHA PARTICLE-INDUCED TORQUE

OFMC is employed to study the alpha particle-induced torque profile formed in a Normal Shear (NS), a Weakly Reversed Shear (W-RS) and a Reversed (negative) Shear (RS) configuration. These equilibria are designed to apply for SlimCS plasmas and are obtained by solving the Grad-Shafranov equation numerically using the equilibrium code MEUDAS [18], with the same pressure profile $p(\psi)$ used in each case. The chief parameters of SlimCS plasmas are as follows: the major radius $R = 5.63$m, the minor radius $a = 2.1$m, the toroidal magnetic field $B_\phi = 6.0$T, the plasma current $I_p = 16.7$MA, ellipticity $\kappa = 2.1$ and triangularity $\delta = 0.4$. In general, it is hard numerically to find the equilibrium of a DEMO plasma with both a strong RS and ITBs at the same time. Only in this section, as inputs for OFMC, do we use density and temperature profiles with ITBs that are not identical to the pressure profile used in the equilibrium solver; rather, this approach is advantageous because we easily can understand the physical origin of the observed results by varying a pressure profile or magnetic shear individually. We then focus on the physics of the impact of the magnetic configuration on the behaviour of alpha particles.

The safety factor q profiles corresponding to the NS, W-RS and RS configurations are shown in figure 2. A strong RS configuration may not be realistic for a DEMO plasma. Nevertheless, it is useful to study the behaviour of alpha particles running through a low B_θ region. OFMC follows 400,000 test particles until they slow down. Details of how to numerically deal with alpha particles in OFMC are found in Ref. [7]. Figure 3 displays the profiles of the collisional and $\vec{j} \times \vec{B}$ torques and their total as well as the source profile of alpha particles S that depends on the background density and temperature profiles. Shared characteristics among the three cases include: (1) a co-directed collisional torque and a counter-directed $\vec{j} \times \vec{B}$ torque appear over the entire region; (2) both torques cancel each other out over the entire profile, i.e., no net torque; (3) both torques rapidly diminish outside the ITB; and (4) the location of the maximum magnitude of both torques is nearly identical to that of the maximum gradient of S. In contrast, a clear difference among the three cases is that the magnitude of the cocollisional and counter $\vec{j} \times \vec{B}$ torques is different for each case. We will carefully consider these points in the following.

The preceding studies and our simulations regarding particle orbits, both confirm an excess of co-directed particles because co-collisional torque appears over the entire region. We first focus on the region near the magnetic axis, where the low gradient of the source profile is observed compared to that of the other regions and, in addition, where the q profile is quite different, for the three cases. Under the collisionless assumption, we carry out an orbit-following simulation during a one bounce period to clarify how alpha particles behave due to the influence of the magnetic shear. Because we assume for this case only a collisionless plasma with no ripple field, all test particles must return to where they were born, with their orbits closed in a bounce. In doing so, after following the orbits of all test particles during a bounce period, we are able to count exactly the number of test particles categorized as co or counter and as passing or trapped. We note that even though a collisionless plasma is just an assumption for this purpose, a burning plasma will be almost collisionless due to its very

high temperature. Figure 4 shows the ratio of counter- and co-passing test particles to their total at birth for the (a) NS and (b) RS configurations, inside r/a = 0.2. In both cases co-passing particles actually outnumber counter-passing ones, but in case (b) the ratio of co- to counterpassing particles is larger than that in case (a) for almost every region. Subsequently, we deduce that collisional slowing-down and pitch-angle scattering processes do not create asymmetry in the co- and counter-directions, but that magnetic topology does. This finding also can be readily confirmed by drawing collisionless orbits of particles with various pitch angles in the RS configuration, as shown in figure 5. When focusing on the orbits of particles born on the $\psi = 0.01$ surface on the Low-Field-Side (LFS), we find that particles with co-directed pitch angles at birth are confined inside $\psi \approx 0.01$, as shown in figure 5 (a), while some of those with counter-directed pitch angles drift across the $\psi = 0.1$ surface, as shown in figure 5 (b), because they are no longer passing particles, but trapped particles with wide orbit widths due to the nearly-unchanged along their trajectories. In contrast, particles with co-directed pitch angles born on the High-Field-Side (HFS) tend to move outward from the surface of their birth, and those with counter-directed pitch angles tend to go inward, as shown in figures 5 (c) and (d). Some of the counter particles become trapped all the same. In summary, when we focus on the balance of particles born at $\psi = 0.01$ within $\psi = 0.1$, a slight imbalance in the direction of co and counter particles produces a co bias for passing particles and a counter bias for trapped ones. Accordingly, we confirm that the magnetic field creates an asymmetry for both passing and trapped particles and a negative magnetic shear enhances this tendency. This is also the case in the NS configuration, but to a lesser extent: co-passing particles outnumber counter-passing ones, and co particles are rarely trapped, compared to counter ones. Schneider et al. in a straightforward manner explain the reason for the excess of co-passing particles in the current-hole configuration, using the concept of the conservation of toroidal angular momentum [5].

We should be careful not to conclude that these results readily lead to the dominance of co-collisional and counter $\vec{j} \times \vec{B}$ torques. Such may not be the case because many of the alpha particles born outside $\psi = 0.1$ enter the region within $\psi = 0.1$, influencing torque deposition, and subsequently there is a possibility that some of them may act in a manner that weakens or even cancels such tendencies. In figure 3, the source profiles S_α were all parabolic, i.e., they had more or less a finite gradient over all profiles. In order to accentuate the effects of a finite gradient of S_α, next we artificially assume that the profile of S_α is flat in the core region and steep in the edge region, i.e., a box-type profile. We carry out simulations with the same conditions as in figure 3 except for S_α. We expect that both the collisional and $\vec{j} \times \vec{B}$ torques will be prominent near the region where S_α is steep and be small elsewhere, provided that the gradient of S_α causes both torques in figure 3 to increase in magnitude. The simulation results are exhibited in figure 6, clearly showing that for all cases, collisional torque as well as the $\vec{j} \times \vec{B}$ torque is negligible in the central region where $0 \leq r/a \lesssim 0.6$. Regions with a steep S_α gradient coincide with those of prominent collisional and $\vec{j} \times \vec{B}$ torques. The relative absence of any collisional torque in the central region indicates that collisional torque is offset by the isotropy of alpha particle generation, as expected from the earlier consideration. As

seen in (6), the $\vec{j} \times \vec{B}$ torque is proportional to $B_\theta \propto \partial\psi/\partial\bar{\rho}$. Of course, the $\vec{j} \times \vec{B}$ torque depends on the trajectories of fast particles, but basically, this B dependence tends to diminish the $\vec{j} \times \vec{B}$ torque in the negative shear region in reversed shear configurations. As a result, both collisional and $\vec{j} \times \vec{B}$ torques may not be significant in the region where the S_α profile is flat.

We, in turn, consider the mechanisms for generating the torques due to the S_α gradient. For collisional torque, Tani and Azumi explained the mechanism of the excess of co-passing particles owing to the gradient of S_α, using a simple schematic diagram of alpha particle trajectories, as shown in figure 6 in Ref. [7]. In short, when a pair of passing particles with co and counter velocities passing through a certain point in a plasma is considered, it is found that the co particle goes through the inner region where more alpha particles are born, while a counter particle goes through the outer region where fewer are born. This fact leads to the dominance of co-passing particles at each radial position. Next, in order to identify why the gradient of S_α produces a counter $\vec{j} \times \vec{B}$ torque, we should focus on the trapped orbits in the corresponding regions. Figure 7 shows co- and counter-trapped orbits born at $\psi = 0.4$ and those at $\psi = 0.5$. We imagine a situation in which there is a steep gradient of S_α between these surfaces. For example, let us assume that 100 test particles are generated at the point denoted by a cross in figure 7, and 10 test particles at the point denoted by an open square, based on speculation using the S_α profile in the figure. In the case in which co-trapped and counter-trapped particles are equally generated at both points, counter-trapped particles born at the cross symbol move outward in the region between the $\psi = 0.4$ and 0.5 surfaces, while co-trapped particles born at the open square symbol move inward in the same region. These contributions cancel each other, and a net 45 test particles moves outward, producing an outward fast-ion radial current. An inward ion radial current flowing in the opposite direction subsequently creates a $\vec{j} \times \vec{B}$ torque that drives counter rotation in the plasma. In practice, the fact that there are to a certain extent more counter-trapped particles generated than co-trapped ones, as already noted, reinforces a counter $\vec{j} \times \vec{B}$ torque.

5. ESTIMATION OF TORQUE AND TOROIDAL ROTATION IN SLIMCS PLASMAS

5.1. ALPHA PARTICLE-INDUCED TORQUE

We estimate the torque induced by alpha particles and the resulting toroidal rotation in SlimCS plasmas. Equilibria in the NS and W-RS configurations are constructed using the ACCOME code [19] that is able to solve the Grad-Shafranov equation consistent with arbitrarily given density and temperature profiles and a current density profile driven by several current-drive methods. As already noted in section 1, a 0.5–1.5MeV tangential NBI of 50MW will be installed in SlimCS and may constitute the sole heating system capable of effectively driving rotation. Therefore, we also will show calculation results with the net torque input of NBIs for three different injection energies of 0.5, 1.0 and 1.5MeV: these net torque values will provide a measure of the degree of impact of an alpha particle-driven torque. The given pressure profiles and the resultant q profiles are exhibited in figure 8 (b), and the simulation results regarding the alpha particledriven torque are shown in figure

8 (a) for both cases. The net torque input of alpha particles as well as the NBIs is summarized in table 1, showing that for (a) the NS and (b) the W-RS cases virtually no net torque emerges because both torques cancel each other out almost exactly. The overall tendencies of torque profiles seem to be similar to those in figure 3. In fact, for both cases, the collisional and $\vec{j} \times \vec{B}$ torques nearly cancel each other out and their profiles are similar. However, we clearly found that each torque for the W-RS case was amplified inside r/a $\approx$ 0:55, compared to that for the NS case, as seen in figure 8 (a). This finding would not seem to be due to the difference in the S gradient, because in this example the S gradient in the NS case resembles that in the W-RS case, although the q profiles are different, as shown in figure 8 (b): the only clear difference in the simulation settings is the q profile. As described in the previous section, a flat S profile scarcely produces any significant torque, regardless of q profiles. For these cases, we have a finite S gradient over the entire region, implying that we have finite collisional and $\vec{j} \times \vec{B}$ torques. Figure 8 (a) evidently demonstrates that under this circumstance, negative magnetic shear enhances collisional and $\vec{j} \times \vec{B}$ torques. As shown in figure 4, we have confirmed that the number of co-passing particles in the RS configuration is larger than that in the NS configuration. Accordingly, the co-collisional torque becomes stronger in the former case, provided that the S gradients are identical. This is also the case for trapped particles. Figure 8 (c) shows that the ratio of counter- and co-trapped particles relative to all trapped particles at birth inside r/a = 0.3. When comparing the ratio for the NS case to that for the W-RS case, we apparently find that the number of co-trapped particles in the W-RS configuration is smaller than in the NS configuration. More counter-trapped particles tend to create a larger, negative $\vec{j} \times \vec{B}$ torque. These effects vanish outside r/a $\approx$ 0.55 where the same q profile appears for both cases. We again state that this enhancement effect of the magnetic shear may arise in a region with a finite S gradient. A breakdown of the characteristics of test particles in the W-RS case is given in detail in ??.

As summarized in table 1, even though the contribution of each to the total torque is comparable or divergent at most by a factor of three for the alpha-driven and NBIdriven cases, alpha-driven torque does not become significant due to cancellation. We believe that this finding conforms to the conservation of toroidal angular momentum.

5.2. NBI-INDUCED TORQUE

The radial profiles of NBI-induced torque for the 0.5, 1.0 and 1.5MeV cases, corresponding to cases (c), (d) and (e) in table 1, respectively, are shown in figure 9. Table 1 would seem to indicate that we should choose the 0.5MeV NBI to maximize the net torque input. However, as shown in figure 9, the beam particles of 0.5MeV cannot sufficiently penetrate into the core region of a SlimCS plasma and tend to be deposited in the outer region. From the standpoint of the efficiency of Neutral Beam V Current Drive (NBCD), which is a separate important role of NBI, a 0.5MeV NBI will not be optimal, because an NBI with higher energy can drive the current more efficiently. In fact, OFMC calculations show parallel beam-driven currents of 4.067MA, 5.074MA and 5.512MA using 0.5MeV, 1.0MeV and 1.5MeV NBIs, respectively, in our settings. In contrast to the 0.5MeV NBI, we obtain a centrally-

peaked torque profile using the 1.5MeV NBI, while the net torque diminishes. Considering also an engineering point of view, we believe that an NBI with 1.0MeV or slightly higher energy is the most promising choice for DEMO reactors. The torque profile using the 1.0MeV NBI is modestly peaked, and subsequently the NBI drives toroidal rotation more uniformly across the region. We, therefore, may deduce that alpha-driven torque will not become very significant in DEMO plasmas using a tangential NBI.

5.3. ESTIMATING TOROIDAL ROTATION DRIVEN BY ALPHA-INDUCED TORQUE

The multi-fluid transport code TASK/TX is a 1D transport code to calculate selfconsistently the evolution of a plasma, including the radial electric field and rotations [9]. Utilizing this code together with the torque profiles calculated by OFMC, for both cases we now roughly estimate a toroidal rotation profile driven solely by alpha particleinduced torque, without NBIs. We assume that momentum diffusivity is equivalent to the thermal diffusivity calculated by the CDBM model [20] and neglect momentum convection, for the sake of simplicity. Time-dependent simulations in a steady state are carried out to obtain the toroidal rotation of a burning plasma with the density, temperature and current density profiles used by ACCOME.

Toroidal rotation profiles in a nearly steady state in SlimCS are shown in figure 10 for the NS and W-RS cases: the rotation profiles almost reach a steady state at t = 1s with the temperature profiles fixed and the density profile nearly unchanged. In both the NS and W-RS configurations, the plasma attains a modest toroidal rotation up to 10 km=s and rotation shear. However, except for the region near the magnetic axis where the statistical error for collisional torque becomes relatively large, a rotation velocity up to a few km/s may not seem significant. Experimental breakthroughs regarding Resistive Wall Modes (RWMs) demonstrate that an observed threshold of toroidal rotation sufficient to stabilize RWMs is around 0.3% of the Alfvén velocity v_A [21, 22]. In our cases, $v_A \approx 6.33 \times 10^3$ km/s in the core region, 0.3% of which is equal to 19.0km/s. Focusing on the velocity at the outer surface where q = 2, we find negligible rotation velocity, as shown in figure 10, which is far below the threshold level. This finding means that the assistance of NBI and/or any other intrinsic torque source will be required to obtain toroidal rotation sufficient to stabilize RWMs.

CONCLUSIONS AND DISCUSSION

We have numerically investigated the torque driven by alpha particles and the resultant toroidal rotation in SlimCS plasmas, using the OFMC and TASK/TX codes. OFMC can deal with fast particles including fusion-born alpha particles and is now capable of estimating the $j \times B$ torque as well as collisional torque. Although alpha particles are isotropically born overall, their passing component has intrinsic asymmetry in the coand counter-directions due to finite orbit widths; a similar case holds for their trapped counterparts. This asymmetry is due to the magnetic field, and this fact was confirmed by counting co- and counter-passing particles and drawing their orbits based on the proximity of their birth to the magnetic axis. It is found that the gradient of the source

profile of alpha particles is a strong driver in generating co-collisional torque and a counter $\vec{j} \times \vec{B}$ torque. Subsequently, we always have co collisional and counter $\vec{j} \times \vec{B}$ torques in burning plasmas, but both torques virtually cancel each other out locally, unless we consider TF ripple effects. The magnitude of each torque is enhanced in the reversed shear configuration compared to the normal shear configuration, provided that the source gradient is finite and identical in each case. SlimCS plasmas in which density, temperature and current density profiles are consistent with equilibria are calculated by the ACCOME code to estimate torque and the toroidal rotation profile. The net torque due to alpha particles is negligible compared to that produced by the tangential NBI of 50MW with three different energies that is planned to be installed in SlimCS. The transport code TASK/TX predicts the profiles of toroidal rotation induced by alpha particles for both the NS and W-RS cases, using the torque profile from OFMC as an input. Estimated toroidal rotation does not meet the threshold velocity for stabilizing RWMs. Rotation above the threshold will be attainable if the NBI is used to assist rotation at a much higher energy level that is possible in current NBIs.

If a TF ripple were considered in simulations, a net counter torque potentially would arise due to the loss and transport of alpha particles, although SlimCS was designed to minimize TF ripple even in the outboard region on the LFS: the maximum ripple amplitude is at most around 0.3% at the plasma surface [2]. The trajectories of trapped particles are strongly modified by TF ripple especially on their banana tip points, while those of passing particles are not significantly affected. In this sense, we expect that only the $\vec{j} \times \vec{B}$ torque is selectively influenced by TF ripple, possibly leading to a net torque. This work will be reported in the near future. Furthermore, the poloidal displacement of banana tip points would influence the loss rate of alpha particles when a finite radial electric field is included in a simulation. Estimation of the radial electric field is attainable through self-consistent coupling of OFMC and TASK/TX. Both a TF ripple and a radial electric field would potentially produce a net torque in a plasma and, hence, should be taken into account for more realistic and comprehensive calculations.

It is, of course, important to estimate, using actual ITER settings, alpha-driven torque and the resultant toroidal rotation in ITER in which we will obtain the first, steady-state burning plasma. For a quantitative prediction of the rotation, however, some physical issues have not yet been incorporated. It is commonly known that there are several kinds of intrinsic torque sources in a thermal plasma that are not directly associated with fast particles. These sources and a beam-driven torque source may play a dominant role in regulating toroidal rotation, compared to alpha-driven torque. In terms of momentum transport, an accurate estimation of momentum convective velocity and diffusivity is indispensable to an accurate prediction of the profile and magnitude of toroidal rotation as well as the radial electric field, and a reliable, theory-based transport model, therefore, is required. These sources and the transport model should be included in future simulations.

ACKNOWLEDGMENTS

The authors are grateful to Dr A. Salmi, Dr J.-S. Lönnroth, Dr V. Parail and Dr N. Oyama for

their help in carrying out benchmark tests under the implementing agreement for Co-operation on Tokamak Programmes (CTP). One of the authors (MH) wishes to express his gratitude to Mr M. Suzuki for numerical assistance and Dr K. Tani and Dr K. Shinohara for fruitful comments. This work was supported by a Grant-in-Aid for Young Scientists (B) (No 22760667) from The Ministry of Education, Culture, Sports, Science and Technology (MEXT).

APPENDIX A. ESTIMATING THE CHARACTERISTICS OF TEST PARTICLES

For the W-RS case in SlimCS given in section 5, investigating a breakdown of the characteristics of test particles may help us to understand the behaviour of fusion-born alpha particles. An orbit-following simulation during a one bounce motion under the assumption of a collisionless plasma can reveal the characteristics of test particles in a manner similar to that in section 4, leading to the results as shown in figure A1. Figure A1 (a) displays the ratio of co and counter test particles relative to all particles, including both passing and trapped particles, clearly implying that alpha particles are born isotropically: they have no preference in terms of the direction in which they move at the moment of their birth. We note that only a marginal number of test particles are born where r/a and 0.7 as seen in figure 8, so we do not consider the edge region.

However, if we focus on which direction a test particle starts to move by considering passing and trapped particles separately, we find a clear anisotropy. As already confirmed in figure 4, passing alpha particles are apt to move in the co-direction rather than the counter-direction, as shown in figure A1 (c), producing co-collisional torque. On the other hand, figure A1 (d) shows that few co-trapped alpha particles are born adjacent to the magnetic axis. This finding is consistent with the results of preceding research [5, 7, 12]. Furthermore, in the negative shear region, i.e., r/a $\lesssim$ 0:3 (see figure 8 (c)), the ratio of co-trapped to counter-trapped particles is obviously small compared to that in any other region, and it hovers at under 50% almost over the entire region. These findings clearly indicate that a counter $\vec{j} \times \vec{B}$ torque must arise overall. Finally, when we see the trapped particle fraction of alpha particles shown in figure A1 (b), we find that the fraction increases as it nears the plasma surface, though it is smaller than that of thermal particles predicted by standard neoclassical theory. For example, one expression for estimating the trapped particle fraction is $f_t = 1.46\epsilon^{1/2} - 0.46\epsilon^{3/2}$ [23]. In this case, the result is ~ 0.7 in the edge region, a value which is much larger than that shown in figure A1 (b), which is at most 0.25. As noted in section 2, because the trapping boundary at high energy is different from that at low energy, we must bear in mind that we cannot apply a formula for estimating the trapped particle fraction of thermal particles to the task of estimating that of alpha particles. In fact, it was found in TFTR experiments that the initial trapped fraction of alpha particles in the RS configuration was less than 30% [24]: the aspect ratio of TFTR is similar to that expected in SlimCS. This observation is qualitatively consistent with our results.

REFERENCES

[1]. Asakura N. et al 1993 Nuclear Fusion **33** 1165

[2]. Tobita K. et al 2007 Nuclear Fusion **47** 892

[3]. Kolesnichenko Y.I. and Yakovenko Y.V. 1990 Fusion Technology **18** 597

[4]. Rosenbluth M.N. and Hinton H.L. 1996 Nuclear Fusion **36** 55

[5]. Schneider M. et al 2005 Plasma Physics and Controlled Fusion **47** 2087

[6]. Thyagaraja A, Schwander F and McClements K G 2007 Physics of Plasmas **14** 112504

[7]. Tani K and Azumi M. 2008 Nuclear Fusion **48** 085001

[8]. Tani K et al 1981 Journal of Physics Soc. Japan **50** 1726

[9]. Honda M and Fukuyama A 2008 Journal of Computational Physics **227** 2808

[10]. Heikkinen J.A. and Sipilä S.K. Computational Physics Communication **76** (1993) 215

[11]. Chu T.K. 1996 Physics of Plasmas 3 3397

[12]. Chiu S.C, Chan V.S. and Omelchenko Y.A. 2002 Physics of Plasmas **9** 877

[13]. Egedal J 2000 Nuclear Fusion **40** 1597

[14]. Hinton F L and Wong S K 1985 Physics of Fluids **28** 3082

[15]. Hinton F L and Rosenbluth M N 1999 Physics Letters A **259** 267

[16]. Honda M, Takizuka T, Fukuyama A, Yoshida M and Ozeki T 2009 Nucl. Fusion 49 035009

[17]. de Vries P C et al 2008 Nuclear Fusion **48** 035007

[18]. Azumi M et al Proc. 4th Int. Symp. on Computational Methods Applied Science Engineering, Paris (North- Holland, Amsterdam, 1980) 335

[19]. Tani K, Azumi M and Devoto R S 1992 Journal of Chemical Physics **98** 332

[20]. Fukuyama A et al 1995 Plasma Physics of Controlled Fusion **37** 611

[21]. Takechi M et al 2007 Physical Review Letters **98** 055002

[22]. Reimerdes H et al 2007 Physical Review Letters **98** 055001

[23]. Kim Y.B, Diamond P.H. and Groebner R.J. 1991 Physics of Fluids B**3** 2050

[24]. Redi M.H. et al 1999 Physics of Plasmas **6** 2826

	col. torque	$\vec{j} \times \vec{B}$ torque	total
(a) NS	10.78	–10.78	$-9{:}69\ 10^{-2}$
(b) W-RS	12.08	–12.20	$-1{:}18\ 10^{-1}$
(c) NBI 0.5MeV	43.52	31.68	75.20
(d) NBI 1.0MeV	37.58	17.31	54.88
(e) NBI 1.5MeV	34.13	11.78	45.90

Table 1. Collisional and $\vec{j} \times \vec{B}$ torques and their total as well as torques produced using NBIs with different injection energies, integrated over the entire volume, in [Nm] units.

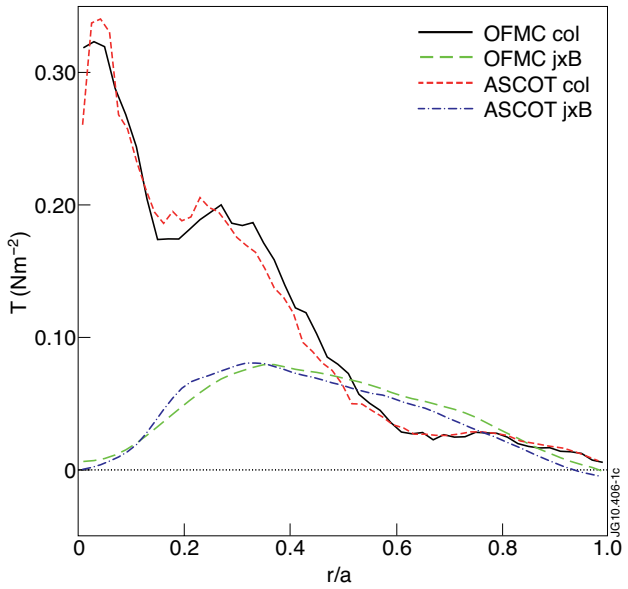

Figure 1: Comparison of the collisional and $\vec{j} \times \vec{B}$ torques estimated by OFMC and ASCOT.

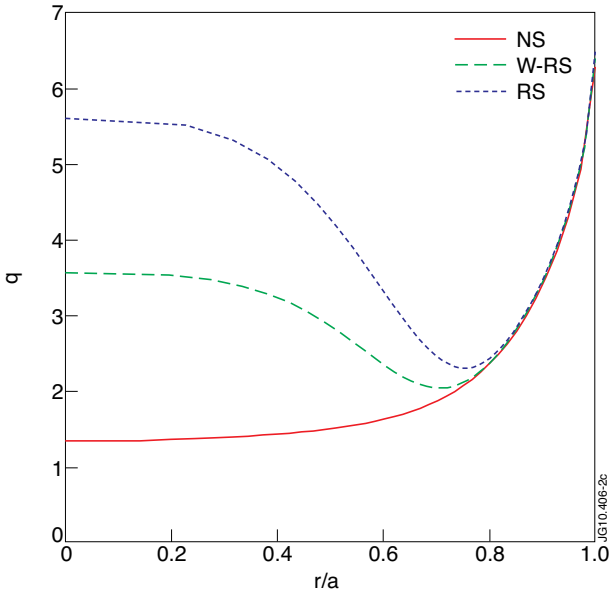

Figure 2: The q profiles in the NS, W-RS and RS configurations calculated by MEUDAS.

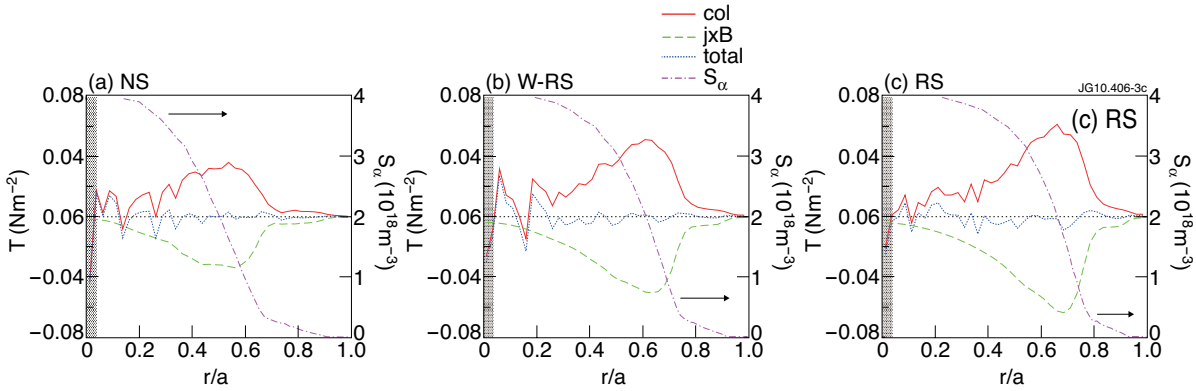

Figure 3: Profiles of the collisional (col) and $\vec{j} \times \vec{B}$ (j×B) torques and their total (total) in the (a) NS, (b) W-RS, and (c) RS configurations. The source profiles of alpha particles (S) are also shown for each case. Hereafter, the hatched region adjacent to the magnetic axis denotes the region where the values seem to be statistically meaningless.

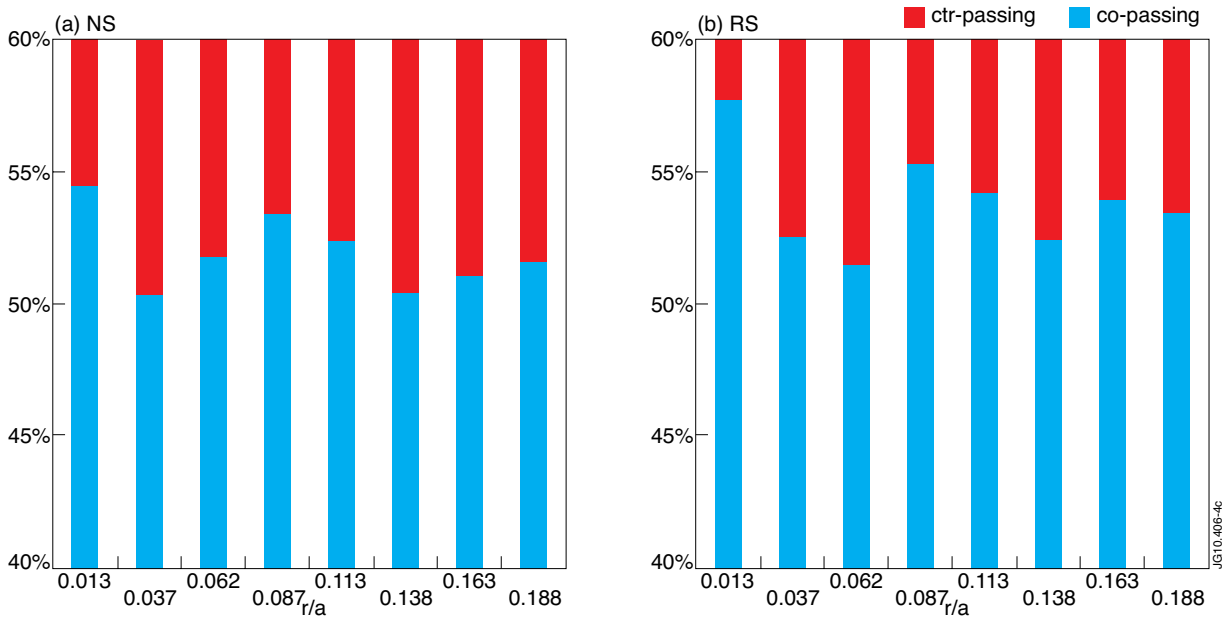

Figure 4: The ratio of counter- and co-passing test particles relative to all passing particles at birth near the magnetic axis in the (a) NS and (b) RS configurations.

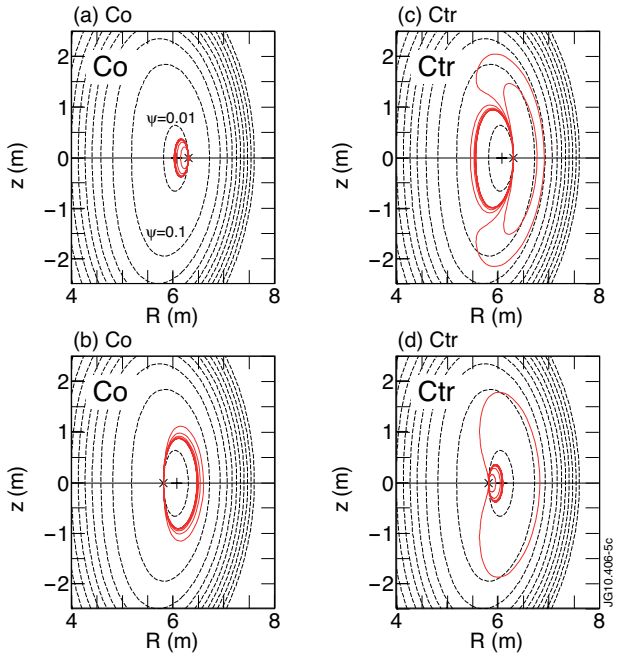

Figure 5: Collisionless orbits of (a) co- and (b) counter-particles born at the midplane of the ψ = 0:01 surface on the LFS of a RS plasma. Cases (c) and (d) are equivalent to cases (a) and (b) except that they are for the HFS, respectively. In each figure eight orbits are drawn with pitch angles from 10^o to 80^o at 10^o intervals for cases (a) and (c) and from 100^o to 170^o for cases (b) and (d).

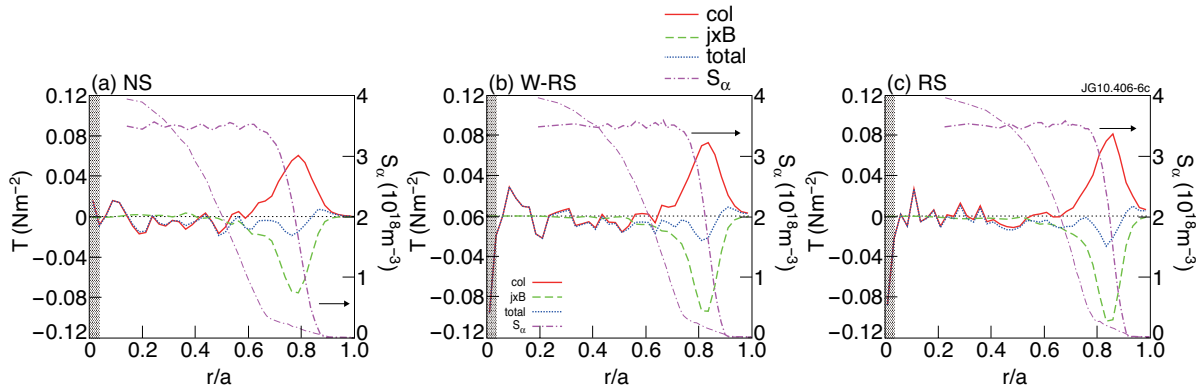

Figure 6: Profiles of the collisional (col) and $\vec{j}\times\vec{B}$ (j×B) torques and their total (total) in the (a) NS, (b) W-RS, and (c) RS configurations with the S profiles artificially held flat in the core and precipitous in the edge regions.

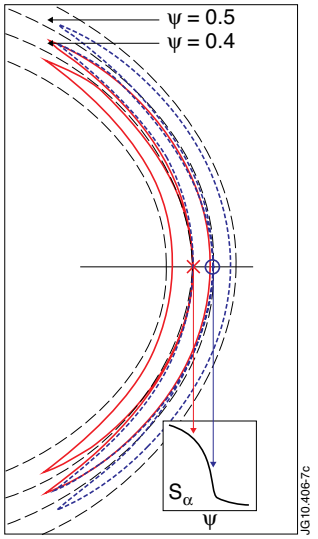

Figure 7. Trapped orbits born at ψ = 0.4 (solid lines) and those born at ψ = 0.5 (dotted lines). The lower right figure shows a schematic drawing of the steep S profile. The horizontal scale of the figure has been doubled.

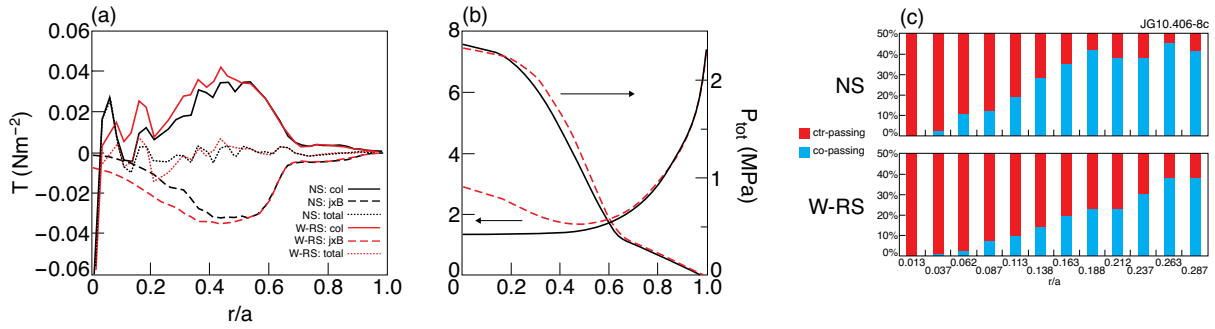

Figure 8: (a) Profiles of the collisional (col) and $\vec{j}\times\vec{B}$ (j×B) torques and their total(total) in the NS and W-RS configurations in SlimCS. (b) Profiles of the corresponding q and the pressure Ptot. In figures (a) and (b), the black thin lines correspond to the NS case and the red thick lines, the W-RS case. (c) The ratio of counter- and co-trapped test particles relative to all trapped particles at birth near the magnetic axis for the NS and W-RS cases.

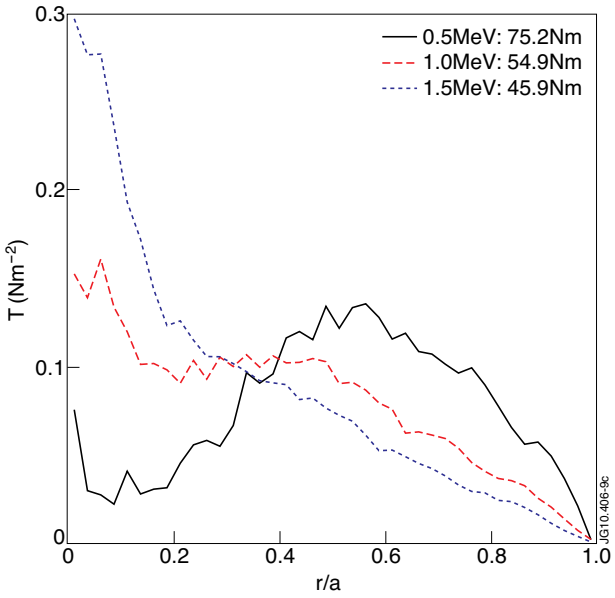

Figure 9: Profiles of total torque produced by NBIs with 0.5, 1.0 and 1.5MeV for the W-RS case.

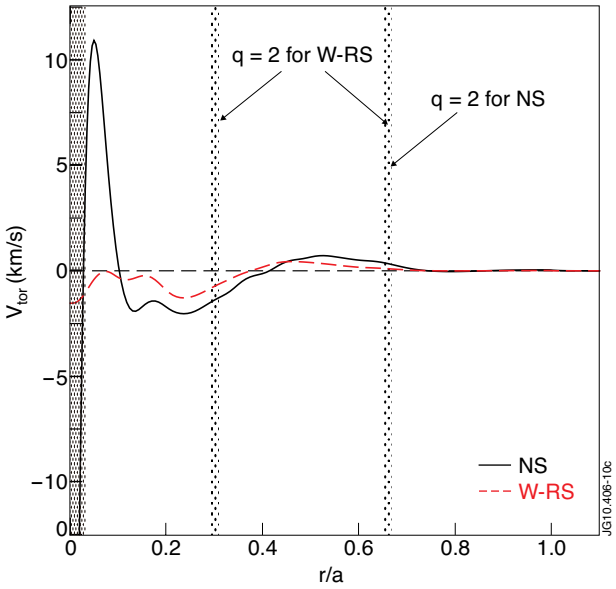

Figure 10: Toroidal rotation profiles for the NS and W-RS cases at t = 1 s after initiation. The densely hatched region adjacent to the magnetic axis denotes the buffer zone where we may not regard the estimated rotation as meaningful, corresponding to figure 8. The hatched regions correspond to the rational surfaces where q = 2.

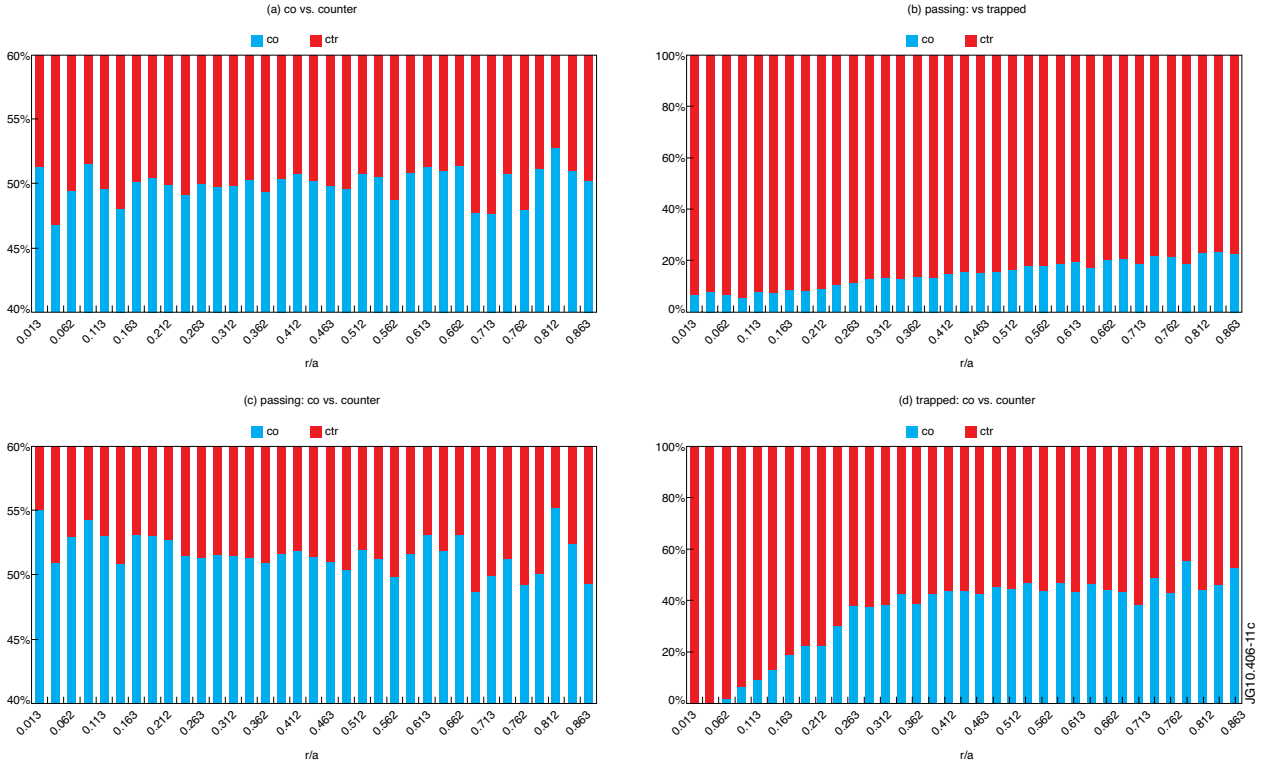

Figure A1. The ratio of co and counter test particles relative to (a) all particles, including both passing and trapped particles, (c) all passing particles and (d) all trapped particles in the W-RS configuration. (b) The ratio of passing and trapped test particles relative to all particles.